Design and Analysis of a Magnetless Dual-Mode DC-Excited Multitoothed Switched Reluctance Machine

Christopher H. T. Lee, K. T. Chau, *Fellow, IEEE*, Chunhua Liu, *Member, IEEE*, and Mu Chen
Department of Electrical and Electronic Engineering
The University of Hong Kong, Hong Kong, China
ktchau@eee.hku.hk

***Abstract*—This paper artfully integrates an external DC-field winding and double-rotor (DR) topology into the multitoothed switched reluctance (MSR) machine to form the new DC-excited MSR (DC-MSR) and DR-DC-MSR machines. With the DC-field excitation, all the torque producing zones can be utilized and hence the torque density can be improved. In addition, the independent DC-field winding can effectively control the flux density to achieve the efficiency optimization. Meanwhile, the proposed machines can naturally offer two different operation modes. By using the time-stepping finite-element-method (TS-FEM), the characteristics and performances of the proposed machine at both modes of operation are analyzed and verified.**

***Index Terms*— Reluctance machine, magnetless, multitoothed, DC-field winding, double-rotor, dual-mode operation.**

I. Introduction

Permanent magnet (PM) machines can offer better torque performances and thus these types of machine have been actively developed [1], [2]. However, the prices of the PM materials have risen rapidly; and therefore the advanced magnetless machines which contain the cost benefits become more and more attractive [3].

The purpose of this paper is to integrate the concepts of external DC-field and double-rotor (DR) topology into multitoothed switched reluctance (MSR) machine to form the flux controllable, high torque density, magnetless DC-MSR and DR-DC-MSR machines. In addition, the proposed machines can operate at two different operation modes, namely doubly salient DC (DSDC) mode and MSR mode. By applying the time-stepping finite element method (TS-FEM) [4], [5]; the machine designs will be verified and compared.

II. Machine Design

Fig. 1 shows the topologies of the DC-MSR and DR-DC-MSR machines. The machines consist of the stators of 6 salient poles, each fitted with 4 teeth, and resulting 24 equivalent stator teeth. Meanwhile, the rotors have 22 salient poles. The proposed machines adopt two kinds of windings, namely the armature and DC-field windings. The major distinction of both machines comes from the DR topology.

The key design data of the machines is shown in Table I and the key features are summarized as:

- Without installation of any PM materials, both machines take the definite merit of cost benefit.
- With the multitoothed structure, they can offer the flux-modulation effect to boost up the torque density.
- By utilizing the independent DC-field excitation, all torques producing zones are utilized. The airgap flux density can also be controlled effectively for efficiency optimization.
- With different conduction schemes, both machines can naturally achieve two operation modes, namely the DSDC mode and MSR mode.
- When there is any open circuit fault at the DC-field excitation, the machines can immediately switch to the MSR mode to maintain the torque performances.
- The inner spacing of the DR-DC-MSR machine is utilized to serve as the inner rotor to further boost up its torque density.

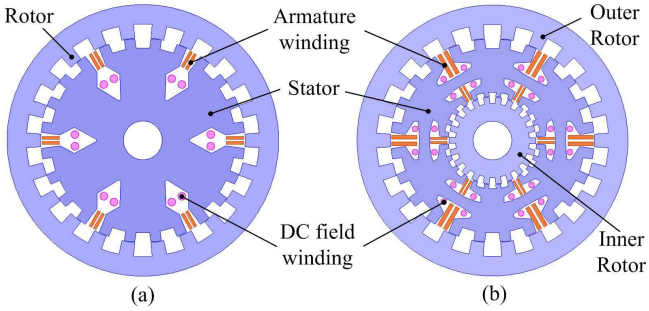

Fig. 1. Proposed machines: (a) DC-MSR machine. (b) DR-DC-MSR machine.

III. Analysis Approach

To describe the machine modeling, TS-FEM is applied and three sets of equations are established. First, the electromagnetic field equation is governed by [4], [5]:

$$\Omega: \frac{\partial}{\partial x}\left(\nu\frac{\partial A}{\partial x}\right)+\frac{\partial}{\partial y}\left(\nu\frac{\partial A}{\partial y}\right)=-J-\nu\left(\frac{\partial B_{ry}}{\partial x}-\frac{\partial B_{rx}}{\partial y}\right)+\sigma\frac{\partial A}{\partial t} \quad (1)$$

where Ω is the field solution region, A the magnetic vector potential, J the current density, σ the electrical conductivity, and the B_{rx}, B_{ry} remnant flux density. Second, the armature circuit equation of the machine during motoring is given by:

$$u = Ri + L_e\frac{di}{dt}+\frac{l}{s}\iint_{\Omega_e}\frac{\partial A}{\partial t}d\Omega \quad (2)$$

where u is the applied voltage, R the winding resistance, L_e the end winding inductance, l the axial length, s the conductor area of each turn of per phase winding, and Ω_e the total cross-sectional area of conductors of each phase winding. Third, the motion equation of the machine is given by:

$$J_m\frac{\partial\omega}{\partial t}=T_e-T_L-\lambda\omega \quad (3)$$

where J_m is the moment of inertia, ω the mechanical speed, T_L the load torque, and λ the damping coefficient.

IV. Result

By performing the TS-FEM, the no-load electromotive forces (EMFs) of the proposed machines at rated speed versus the DC-field excitations are shown in Fig. 2. Firstly, it can be observed both machines perform similarly and their no-load

EMFs increase with the DC-field excitation. These validate that the proposed machines can strengthen or weaken the flux densities by regulating the DC-field currents in order to achieve the efficiency optimization. Meanwhile, due to the double windings structure, the no-load EMFs of DR-DS-MSR machine is larger than its counterpart.

Secondly, the torque performances at steady stage of the DC-MSR and DR-DC-MSR machines are as shown in Fig. 3 and 4, respectively. It can be observed that the average steady torques of DC-MSR machine at DSDC and MSR modes are 15.3 Nm and 15.8 Nm, respectively; meanwhile, of DR-DC-MSR machine of both rotors are 20.3 Nm and 20.1 Nm, respectively. These confirm that both machines can reach the same torque levels at two different modes. However, the MSR modes require the larger armature currents and also result with larger torque ripples. Therefore, MSR modes should act as the fault-tolerant operations. Furthermore, with the DR structure, DR-DC-MSR machine outperforms its counterpart.

Thirdly, the core losses of the machines are as shown in Fig. 5. The average core losses of DC-MSR machine at DSDC and MSR modes are 17.2 W and 20.4 W, respectively; meanwhile, of DR-DC-MSR machine are 26.4 W and 35.2 W, respectively. The core losses at different modes illustrate different patterns due to the fact that both of them are operated under different principles. Meanwhile, DSDC modes of both machines obtain slightly lower core loss than its counterparts.

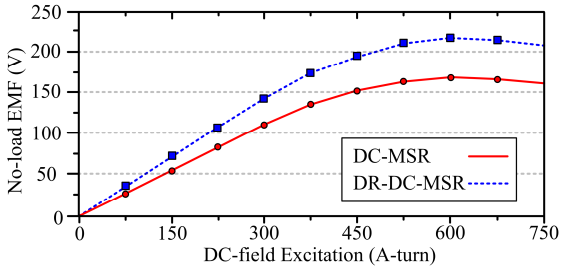

Fig. 2. No-load EMFs versus DC-field excitations.

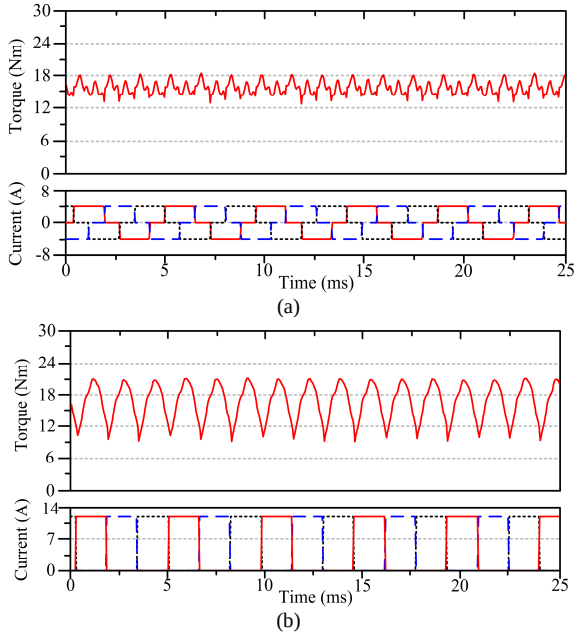

Fig. 3. Torque waveforms of DC-MSR: (a) DSDC mode. (b) MSR mode.

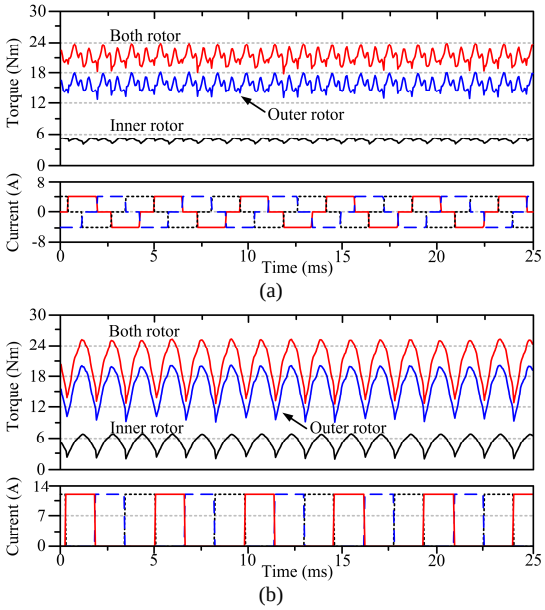

Fig. 4. Torque waveforms of DR-DC-MSR: (a) DSDC mode. (b) MSR mode.

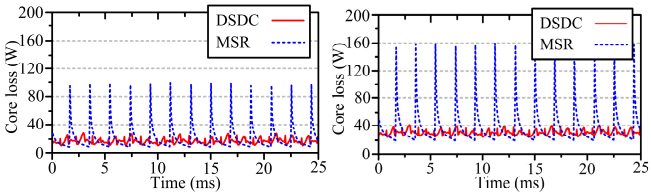

Fig. 5. Core losses: (a) DC-MSR machine. (b) DR-DC-MSR machine.

TABLE I. KEY DATA OF PROPOSED MACHINES

Item	DC-MSR	DR-DC-MSR
Outer rotor outside diameter	280.0 mm	280.0 mm
Outer rotor inside diameter	211.2 mm	211.2 mm
Stator outside diameter	210.0 mm	210.0 mm
Stator inside diameter	40.0 mm	91.2 mm
Inner rotor outside diameter	N/A	90.0 mm
Inner rotor inside diameter	N/A	40.0 mm
Air-gap length	0.6 mm	0.6 mm
Stack length	80.0 mm	80.0 mm

V. Acknowledgement

This work was supported by a grant (Project No. HKU710612E) from the Hong Kong Research Grants Council, Hong Kong Special Administrative Region, China.

References

[1] Z. Q. Zhu, and D. Howe, "Electrical machines and drives for electric, hybrid and fuel cell vehicles," *Proceedings of IEEE*, Vol. 95, No. 4, pp. 746-765, April 2007.

[2] Y. Amara, G. Barakat, and P. Reghem, "Armature reaction magnetic field of tubular linear surface-inset permanent-magnet machines," *IEEE Trans, Magn*., vol. 47, no. 4, pp. 805-811, Apr. 2011.

[3] C. H. T. Lee, K. T. Chau, C. Liu, D. Wu, and S. Gao, "Quantitative comparison and analysis of magnetless machines with reluctance topologies," *IEEE Tran. Magn*, vol. 49, no. 7, Jul. 2013.

[4] J. Faiz, B. M. Ebrahimi, B. Akin, and H. A. Toliyat, Comprehensive eccentricity fault diagnosis in induction motors using finite element method," *IEEE Tran. Magn*., vol. 45, no. 3, pp. 1764-1767, Mar. 2009.

[5] S. Niu, S. L. Ho, W. N. Fu, and J. Zhu, "Eddy current reduction in high-speed machines and eddy current loss analysis with multislice time-stepping finite-element method," *IEEE Tran. Magn*., vol. 48, no. 2, pp. 1007-1010, Feb. 2012.